Research Article Vol. 60, No. 29 / 10 October 2021 / Applied Optics 9213

Use of multiple light sources to enhance the resolution of point light source displays

GANBAT BAASANTSEREN, YULIAN CAO, AND NOMIN-ERDENE DALKHAA*

Department of Electronics and Communication Engineering, National University of Mongolia, Ulaanbaatar 14200, Mongolia
**Corresponding author: nomin-erdene@seas.num.edu.mn*

Received 28 July 2021; revised 21 September 2021; accepted 22 September 2021; posted 22 September 2021 (Doc. ID 438873); published 8 October 2021

The point light sources (PLSs) of integral imaging displays have a wide depth range; however, the resolution is very low. We developed resolution-enhanced PLS displays using multiple light sources that create extra PLSs in the PLS plane. Given aberrations in the lens arrays, the PLSs initially appeared on planes and at distances that differed from the theoretical values. We thus determined the distances between adjacent light sources that compensated for the aberrations. Experimentally, our method enhanced the resolution fourfold compared to that of a conventional PLS display in both vertical and horizontal directions. Our approach allows facile compensation of lens array aberrations and is applicable to 3D displays.

https://doi.org/10.1364/AO.438873

1. INTRODUCTION

Among the various types of 3D displays [1,2], integral imaging (INIM) displays have certain advantages that include full parallax, natural depth perception, full color, continuous viewing, real-time adjustment [3,4], and a simple structure [5–8]. Disadvantages include a narrow viewing angle, low depth range, and low resolution [9–13]. INIM point light source (PLS) displays have a wide depth range [5,14], but the resolution remains low. Resolution depends on the distance between adjacent PLSs [5]. In a conventional PLS display, this distance is equal to the pitch P_L of the elemental lens. For example, if the pitch is 1 mm, the distance between PLSs is also 1 mm, which is very large compared to that of 2D displays. The most important feature of a PLS display is the wide depth range [5,14]. However, the resolution of 3D PLS displays is poor. In this study, we aimed to enhance the resolution.

Park *et al*. developed a 3D/2D convertible display [15]. An additional lens array enhanced PLS resolution, and a polymer-dispersed liquid crystal was used to switch between 3D and 2D modes (PDLC on: 3D; PDLC off: 2D). The additional lens array creates the first PLSs. Each elemental lens of the second lens array creates two PLSs. There are twice as many PLSs as a conventional PLS display; the resolution is thus enhanced twofold.

Alam *et al*. used a scanning mirror and composite lens array with nine Fresnel lenses [16]. A high-speed digital micromirror reflected nine sets of directional elemental images (EIs) into the composite lens. There were three times as many PLSs as for a conventional PLS. The resolution was thus enhanced threefold both vertically and horizontally. However, the mechanical mirror required time for multiplexing.

Wang *et al*. introduced a new system without moving parts [17]. Additional light sources created extra PLSs at the boundaries of two elemental lenses and the maximum resolution was enhanced twofold. However, the additional PLSs did not precisely align with the boundaries because of the effect of Petzval curvature [18–20].

Batbayar *et al*. the nine light sources used to enhance the viewing angle 2.6 times [21]. Due to the aberration of the elemental lens, the light fields overlap, so this method creates duplicated images in some of the viewing fields.

Previous methods enhanced the parameters of the PLS display. However, those methods did not suggest compensating the aberration. Here, we report what we believe, to the best of our knowledge, is a new method to compensate for the aberration of the elemental lens without moving parts. The resolution is determined by the inverse of the distance between adjacent PLSs, so we used additional light sources to reduce the distance between adjacent PLSs. We changed the distances between light sources to compensate for the lens array aberration. Our method is simple and applicable for 3D displays.

2. NEW METHOD

A. PLS Display

The structure of a conventional PLS display is shown in Fig. 1(a). The lens array consists of many small elemental lenses. A light source is placed at the focal point of a collimating lens; parallel light rays emerge from the other side and converge at the focal points of elemental lenses on the PLS plane. The distance between two adjacent PLSs corresponds to the pitch of the elemental lens (P_L).

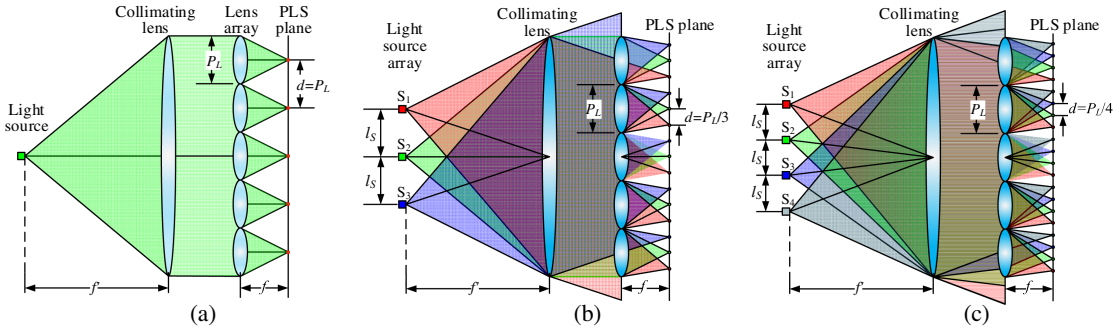

Fig. 1. Principles of (a) a conventional PLS display and our method using (b) three light sources and (c) four light sources.

The resolution of a PLS display [5] is given by

$$R = \frac{1}{d}, \tag{1}$$

where d is the distance between two adjacent PLSs. In Fig. 1(a), $d = P_L$, and the resolution of the conventional PLS display is thus $1/P_L$. Equation (1) shows that the resolution and distance between two PLSs are inversely related. If the distance between two PLSs is reduced, the resolution is enhanced.

B. Our Method

We used additional light sources to reduce the distance between adjacent PLSs, as shown in Figs. 1(b) and 1(c). Additional light sources placed at various distances from the optical axis in the focal plane of the collimating lens are focused at different points in the focal plane of the lens array. This increases the number of PLSs, and thus reduces the distance between adjacent PLSs. We placed, for example, two additional light sources (S_1 and S_3) at a distance l s from the optical axis of the collimating lens, as shown Fig. 1(b). Those light sources create additional PLSs in the PLS plane. Figure 1(b) shows that each elemental lens creates three PLSs; the number of PLSs is thus threefold greater than that of the conventional PLS display. The additional PLSs reduce the distances between adjacent PLSs, and thus enhance the resolution.

Figure 1(c) shows a configuration that enhances the resolution of a PLS display fourfold compared to that of a conventional PLS display. We used four light sources (S_1–S_4) to create additional PLSs in the PLS plane; the distance d between adjacent PLSs is $P_L/4$. In this case, the resolution of our new display and the conventional display are $4/P_L$ and $1/P_L$, respectively [Eq. (1)]; the former resolution is fourfold that of the conventional display. Resolution is enhanced n-fold when the number of light sources is increased $n \times n$-fold in both the vertical and horizontal directions. The most important parameters are the distances between adjacent light sources, the location of the spatial light modulator (SLM), the distances between PLSs, and the elemental image (EI) points.

C. Parameters of the Method

First, the PLS distributions must be uniform. In other words, the distances (d_1–d_3) between neighboring PLSs must be equal in Fig. 2(a). The distance between adjacent PLSs depends on the distance between the two light sources. Basic principles indicate that a ray passing through the collimating and elemental lenses does not change direction. In Figs. 2(b) and 2(c), we use this principle to define the distance between two light sources as

$$l_S = \frac{f' \cdot P_L}{n \cdot f}, \tag{2}$$

where f' is the focal length of the collimating lens, P_L is the pitch of the elemental lens, f is the length of the elemental lens, and n is the -fold resolution enhancement (2, 3, 4, . . .). If n is 3, the resolution is threefold that of the conventional PLS display.

D. SLM Position

Rays from the light source that pass through the collimating and lens arrays are modulated to EI points (h_1–h_5) displayed on the SLM to create the 3D-integrated point P_I, as shown in Fig. 2(b). If the SLM is located on an overlapping PLS light field, an unwanted IMIN point appears. Thus, the SLM is placed on a plane on which PLS light fields do not overlap. There are two possible configurations. The first (SLM_1) is located at the front of the PLS plane. The second (SLM_2) is on the back of the PLS plane, as shown in Fig. 2(a). Some SLM components are not required when displaying the EIs in either configuration. The unused region of SLM_1 (on the front of the PLS plane) is given by

$$h_F = \frac{P_L}{2n-1}. \tag{3}$$

The unused region of SLM_2 (on the back of the PLS plane) is given by

$$h_B = \frac{P_L}{2n+2}. \tag{4}$$

From Eqs. (3) and (4), h_B is smaller than h_F; the SLM2 position is thus better than the SLM_1 position. From Eqs. (3) and (4), the unused region of the SLM is small when n is large. We thus used the SLM_2 position. Figure 2 shows the distance d_s of the SLM from the PLS plane, expressed as

$$d_S = \frac{f}{n+1}. \tag{5}$$

The SLM lies closer to the PLS plane as the resolution increases [Eq. (5)].

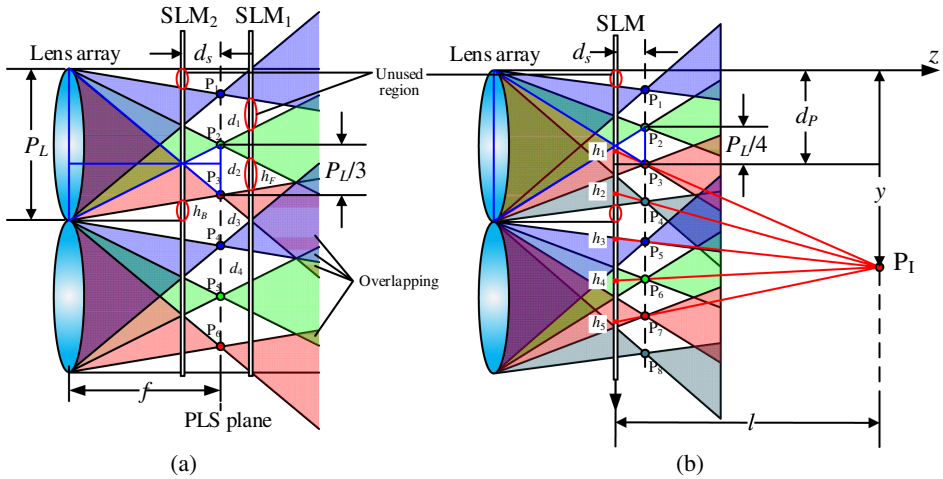

Fig. 2. PLS light fields when (a) three and (b) four light sources are employed.

E. Elemental Images

We used the backward ray tracing method to create EIs. It is the fastest and simplest method to calculate the distances from the EI to the IMIM planes [22,23]. Geometrically, the position of IMIM point P_I is given by

$$y = d_P + (d_P - h)\frac{l + d_S}{d_S}, \tag{6}$$

where h is the y axis coordinate of an EI point, l is the distance of the IMIM point from the SLM, and d_P is the PLS y axis coordinate, given by

$$d_P = P_L\left(\text{ceil}\left(\frac{h}{P_L}\right) - \frac{2(n-k)+1}{2n}\right), \tag{7}$$

where $k = 1 \ldots n$ and ceil function is round toward positive infinity. We determined the parameters of the proposed high-resolution PLS display. However, we must determine some parameters in the experiment because of the optical aberration of the elemental lens.

F. Aberrations of the Elemental Lens

Our lens array has simple plano-convex lenses so optical aberration is inevitable. The aberration of most concern is the Petzval curvature [12,20]. Figure 3 shows a simulation result in which two plane waves are focused on a plano-convex lens with a focal length, diameter, and refractive index of 3 mm, 3 mm, and 1.85, respectively. For an ideal lens, both waves are focused on the focal plane. If the lens is not ideal, the two waves are focused on different planes. The second wave is focused at point B Δz distant from the focal plane and Δy distant from point A. This reduces the distance between two PLSs created by a single elemental lens. Therefore, the PLS distribution becomes nonuniform. Below, we change the distance l_s between two light sources to deal with this problem.

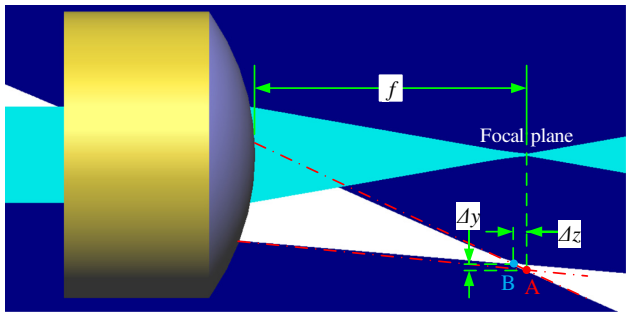

Fig. 3. Plane waves focused on different planes.

3. EXPERIMENTAL RESULTS

We performed two experiments. In the first experiment, we determined the distance between two light sources that compensated for the elemental lens aberration. In the second experiment, we enhanced the resolution three- and fourfold compared to that of the conventional method. Table 1 shows the system parameters.

Figure 4 shows the experimental setup of the display that enhances the resolution fourfold. We soldered 17 surface-mounted LEDs (SMLEDs) to the plate. The middle LED, L1, was used only to adjust the optical setup. LS1–LS16 were employed to increase the number of PLSs.

Table 1. Experimental Specification

Setup	Parameter	Value
SLM	Pitch	0.036 mm (V) × 0.036 mm (H)
	Resolution	1024 × 768
Collimating lens	Type	Achromatic
	Effective focal length	75 mm
	Diameter	50 mm
Lens array	Lens dimensions	1 mm × 1 mm
	Focal length	3.3 mm
Light source	Type	Surface-mounted LED (SMLED)
	Color	White

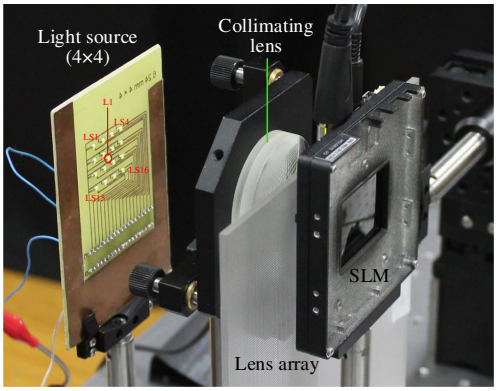

Fig. 4. Experimental setup for the PLS display.

A. PLSs

When the resolution was threefold higher ($n = 3$) than the conventional method, the distances between adjacent PLSs were 7.57 mm [Eq. (2)] and 0.33 mm ($P_L/3$). Nine 3×3 light sources were required to enhance resolution both horizontally and vertically. Many PLS displays use fiber light sources, but these are expensive, large and difficult to set up. Thus, we employed SMLEDs, as follows:

- Prepare a base for the SMLEDs;
- Etch a plate; and
- Solder the SMLEDs to the plate.

We then checked the PLSs. With the camera focused on the PLS plane, Figs. 5(a) and 5(b) show the PLSs of the conventional method and our method, respectively. In Fig. 5(a), the distance between adjacent PLSs is 1 mm because $P_L = 1$ mm. In Fig. 5(b), the number of PLSs is ninefold that of the conventional method. However, the PLS distributions are not uniform. For example, d_1 is 0.28 mm while d_2 is 0.43 mm; the difference is attributable to lens array aberration, as discussed in Section 2.F.

When the distance between adjacent PLS sources was $P_L/3$, we changed that distance and photographed the PLS plane. In Fig. 5(c), the distance between adjacent PLSs is 0.33 mm when the distance between two light sources is $l_S = 8.55$ mm. Experimentally, the PLS distributions were uniform. Thus, the lens array aberrations were compensated when the distance between light sources was 8.55 mm, and it was possible to create 3D images.

When the resolution was fourfold that of the conventional method, the distances between adjacent PLSs were 5.68 mm [Eq. (2)] and 0.25 mm ($P_L/4$). Figures 6(a) and 6(b) show the PLSs of the conventional and new methods, respectively. In Fig. 6(a), the distance between adjacent PLSs is 1 mm because $P_L = 1$ mm. In Fig. 6(b), the number of PLSs is 16-fold higher than for the conventional method. However, the PLS distributions are not uniform. For example, d_1 is 0.21 mm and d_2 is 0.3 mm because of the lens array aberration discussed in Section 2.F.

When the distance between adjacent PLS sources was $P_L/4$, we changed the distance between the two light sources and photographed the PLS plane to measure the distance between adjacent PLSs. As shown in Fig. 6(c), that distance was 0.25 mm when the distance between two light sources was $l_S = 6.24$ mm. Experimentally, the PLS distributions were uniform. Thus, lens array aberrations were compensated when the distance between light sources was 6.24 mm and it was possible to create 3D images.

B. Our PLS Display

From Eq. (5), the SLM distance (d_S value) from the PLS plane is 0.825 mm and 0.66 mm when the resolution is enhanced three- and fourfold, respectively. The SLM is located at the back of the PLS plane [Fig. 2(b)]. The two objects "D" and "S" are 20 and 10 mm, respectively, from the SLM, and the x axis distance between them is 11 mm. We created two sets of EIs using Eqs. (6) and (7), and displayed them on the SLM. We photographed the two objects when the camera was focused on the PLS plane and measured the distance between adjacent PLSs. Figure 7(a) shows the result for the conventional PLS display with one light source; it is difficult to identify "D" and "S" because the resolution is low and the distance between adjacent PLSs is $d = 1$ mm. From Eq. (1), the resolution of the conventional PLS display is $R = 1$ mm^{-1}.

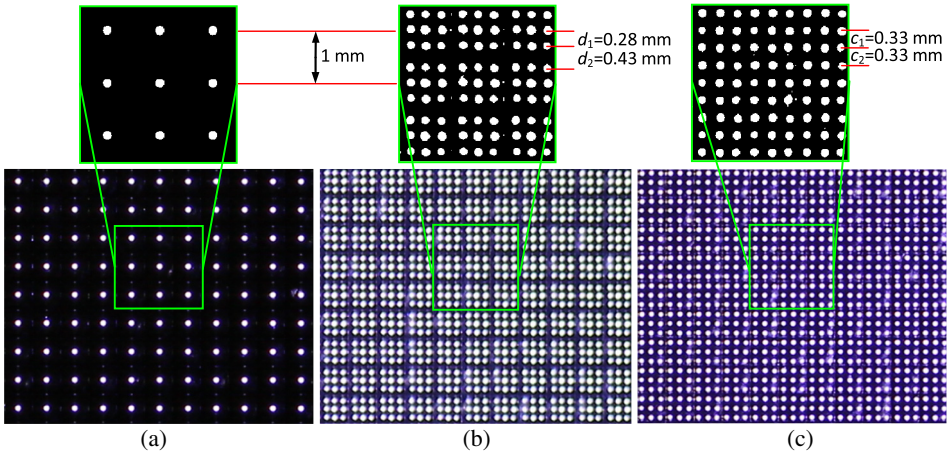

Fig. 5. Photos of the PLS plane of (a) a conventional PLS display and the PLS planes when the distance between two light sources was (b) 7.57 mm and (c) 8.55 mm for $n = 3$ (3×3).

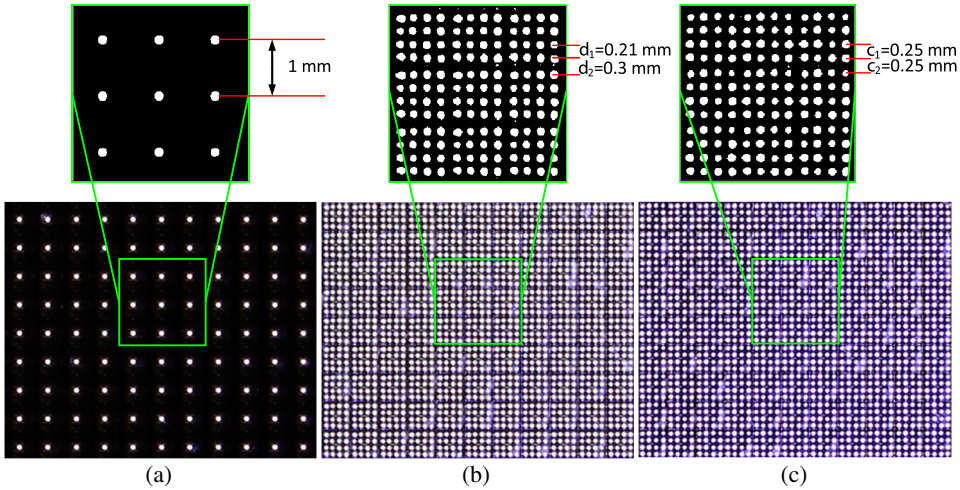

Fig. 6. Photos of the PLS plane of (a) the conventional PLS display and the PLS planes when the distance between two light sources was (b) 5.68 mm and (c) 6.24 mm for $n = 4$ (4×4).

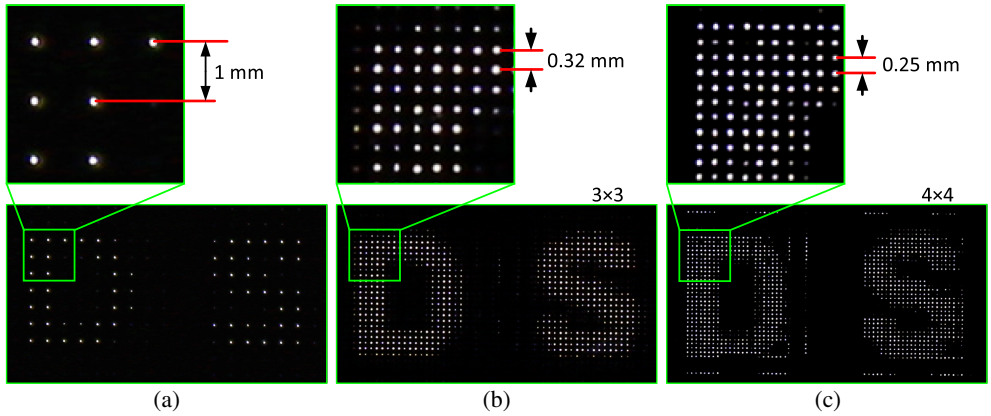

Fig. 7. Experimental results for (a) the conventional PLS display and our PLS displays with threefold (b) and fourfold (c) resolution enhancement.

Figure 7(b) shows the result when 3×3 light sources are employed; "D" and "S" are readily identified because of the additional PLSs; the distance between adjacent PLSs is about $d = 0.32$ mm. From Eq. (1), the resolution now becomes $R = 3.125\ \text{mm}^{-1}$, which represents a threefold improvement over the conventional method. Figure 7(c) shows the result when 4×4 light sources are employed; the distance between adjacent PLSs is about $d = 0.25$ mm. From Eq. (1), the resolution now becomes $\text{R} = 4\ \text{mm}^{-1}$, which represents a fourfold improvement over the conventional method. However, some distortion (inappropriate points) is apparent. The light fields of SMLEDs are different. We cannot solder an SMLED with the exact position and correct directions, so some PLSs have not been captured on camera and some appear in unnecessary positions.

4. CONCLUSION

This study presented high-resolution PLS displays. We used 3×3 and 4×4 light sources to enhance resolution three- and fourfold, respectively. For $n \times n$ light sources, the resolution is enhanced n-fold. The most significant limitation of the INIM display is lens array aberration. We changed the distances between light sources to compensate for this issue. Our simple, inexpensive approach involves the addition of light sources to the focal plane of the collimating lenses for 3D display capability. We are currently working on the removal of inappropriate points.

Funding. National University of Mongolia (P2019-3730).

Disclosures. No author has any conflict of interest.

Data Availability. Data underlying the results presented in this paper are not publicly available at this time but may be obtained from the authors upon reasonable request.

REFERENCES

1. J. Hong, Y. Kim, H. Choi, J. Hahn, J. Park, H. Kim, S. Min, N. Chen, and B. Lee, "Three-dimensional display technologies of recent interest: principles, status, and issues," Appl. Opt. **50**, H87–H115 (2011).
2. J. Geng, "Three-dimensional display technologies," Adv. Opt. Photon. **5**, 456–535 (2013).
3. F. Okano, J. Arai, K. Mitani, and M. Okui, "Real-time integral imaging based on extremely high resolution video system," Proc. IEEE **94**, 490–501 (2006).
4. F. Okano, H. Hoshino, J. Arai, and I. Yuyama, "Real-time pickup method for a three-dimensional image based on integral photography," Appl. Opt. **36**, 1598–1603 (1997).

5. B. Lee, J. Park, and S. Min, "Three-dimensional display and information processing based on integral imaging," in *Digital Holography and Three-Dimensional Display*, T.-C. Poon, ed. (Springer, 2006), Chap. 12.
6. J. Park, S. Min, S. Jung, and B. Lee, "Analysis of viewing parameters for two display methods based on integral photography," Appl. Opt. **40**, 5217–5232 (2001).
7. F. Okano, J. Arai, and M. Kawakita, "Wave optical analysis of integral method for three-dimensional images," Opt. Lett. **32**, 364–366 (2007).
8. S. Park, J. Yeom, Y. Jeong, N. Chen, J. Hong, and B. Lee, "Recent issues on integral imaging and its applications," J. Inf. Disp. **15**, 37–46 (2014).
9. Y. Kim, J. Park, S. Min, S. Jung, H. Choi, and B. Lee, "Wide-viewing-angle integral three-dimensional imaging system by curving a screen and a lens array," Appl. Opt. **44**, 546–552 (2005).
10. L. Yang, X. Sang, X. Yu, B. Yan, K. Wang, and C. Yu, "Viewing-angle and viewing-resolution enhanced integral imaging based on time-multiplexed lens stitching," Opt. Express **27**, 15679–15692 (2019).
11. Ch. Luo, Ch. Ji, F. Wang, Y. Wang, and Q. Wang, "Crosstalk-free integral imaging display with wide viewing angle using periodic black mask," J. Disp. Technol. **8**, 634–638 (2012).
12. Y. Oh, D. Shin, B. Lee, S. Jeong, and H. Choi, "Resolution-enhanced integral imaging in focal mode with a time-multiplexed electrical mask array," Opt. Express **22**, 17620–17629 (2014).
13. L. Zhang, Y. Yang, X. Zhao, Z. Fang, and X. Yuan, "Enhancement of depth-of-field in a direct projection-type integral imaging system by a negative lens array," Opt. Express **20**, 26021–26026 (2012).
14. J. Park, H. Kim, Y. Kim, J. Kim, J. Hong, S. Lee, and B. Lee, "Depth-enhanced three-dimensional–two-dimensional convertible display based on modified integral imaging," Opt. Lett. **29**, 2734–2736 (2004).
15. J. Park, J. Kim, Y. Kim, and B. Lee, "Resolution-enhanced three-dimension/two-dimension convertible display based on integral imaging," Opt. Express **13**, 1875–1884 (2005).
16. A. Alam, G. Baasantseren, N. Kim, and J. Park, "Resolution enhancement of integral-imaging three-dimensional display using directional elemental image projection," J. Inf. Disp. **20**, 221–227 (2012).
17. Z. Wang, A. Wang, X. Ma, F. Ma, and H. Ming, "Resolution-enhanced integral imaging display using a dense point light source array," Opt. Commun. **403**, 110–114 (2017).
18. W. Wallin, "The control of Petzval curvature," J. Opt. Soc. Am. **41**, 1029–1032 (1951).
19. M. Katz, *Introduction to Geometrical Optics* (World Scientific, 2002), pp. 298–300.
20. G. Baasantseren, D. Batbayr, and L. Choimaa, "Effect of Petzval curvature on integral imaging display," Proc. SPIE **9391**, 93911B (2015).
21. D. Batbayar, N. Dalkhaa, M. Erdenebat, N. Kim, and G. Baasantseren, "Point light source display with a large viewing angle using multiple illumination sources," Opt. Eng. **56**, 053113 (2017).
22. Y. Guan, X. Sang, S. Xing, Y. Li, Y. Chen, D. Chen, L. Yang, and B. Yan, "Backward ray tracing based high-speed visual simulation for light field display and experimental verification," Opt. Express **27**, 29309–29318 (2019).
23. T. Oldokh, P. Bold, and G. Baasantseren, "Efficient rendering for elemental image," in *2nd International Conference on Computer Application and Information Processing Technology (CAPIT)* (2014), pp. 97–100.